Chemistry–A European Journal
Research Article
doi.org/10.1002/chem.202404001
Chemistry Europe
European Chemical Societies Publishing
www.chemeurj.org

Amino-Substituted Azoxybenzenes as Potential Redox-Active Catholyte Materials

Dominic Schatz,[a, b] Chris Burdenski,[c] Finn M. Schneider,[a, b] Max M. Hansmann,[c] and Hermann A. Wegner*[a, b]

Aryl diazenes, particularly azobenzenes (AB), represent a versatile class of compounds with significant historical and practical relevance, ranging from dyes to molecular machines, solar thermal and electrochemical storage. Their oxygen-substituted counterparts, azoxybenzenes (AOB), share structural similarities but have been less explored, especially in energy storage applications. This study investigates the redox properties of AOB, comparing them to AB, and evaluates their potential as redox-active materials for energy storage systems. Through cyclic voltammetry (CV) and spectro-electrochemical analyses, we demonstrate that AOBs exhibit a distinct redox behaviour, influenced by the solvent and electrolyte environment, with a reversible oxidation process. Despite their promising redox characteristics, AOBs suffer from capacity decay during galvanostatic cycling, likely due to the instability of the radical cation intermediate. These findings suggest that while AOBs offer intriguing redox properties, further investigation into stabilization strategies are needed for their application in energy storage.

Introduction

Azobenzenes (AB) are gaining attention as versatile active materials for energy storage. Their reversible (*E*)- to (*Z*)-isomerization,[1] and the energy difference between the ground state isomer and the metastable state, are the major foundation for their application as molecular organic solar thermal (MOST) storage systems or as phase change materials.[2] In these storage types, solar energy is stored in the form of bond strains, and is released as heat. A recently established application of ABs for energy storage is their usage in organic batteries due to their reversible reduction. This feature was applied in 2020 by Zhang *et al.* for constructing the first AB redox-flow battery (RFB), in which AB acts as the anolyte.[3] RFBs are a promising technology for large-scale energy storage, especially suitable for grid management with fluctuating energy production from renewables.[4,5] Further improvements based on Zhang's seminal technology increase the operating voltage or transferred the system to an aqueous medium.[6–9] These battery applications are based on the reversible formation of a radical anion, located *inter alia* on the N=N double bond.[10,11] By placement of amino or hydroxyl groups in the *para* positions, an additional reversible $2e^-$ oxidation redox event is realized (Figure 1).[12] Recently, we were able to crystallize the oxidation product by reacting the 4,4′-diethylamine AB with $NOBF_4$, and confirmed the formation of bis-quinone type structure by single crystal XRD.[13] We applied the 4,4′-diethylamino AB as the catholyte in galvanostatic charge/discharge experiments. Although we observed noticeable degradation over multiple cycles, this was the first time AB has been employed as a catholyte.

A structurally akin compound class to AB are azoxybenzenes (AOB). Although AOB are synthetically and structurally similar to their widely utilized counterpart AB,[14] there are only a few applications, e.g. in the field of liquid crystals, polymers[15] and drugs.[16] For AOB, their reductive electrochemical behavior has been comprehensively studied. In aqueous or protic solvents, a $4e^-$ irreversible reduction is observed.[17,18] This reduction leads to the formation of aryl hydrazines, which upon reoxidation provides AB. The removal of oxygen, therefore, represents an irreversible redox process of AOB. In aprotic solvents, the reductive redox chemistry is dependent on the supporting electrolytes.[19] A DMF solution with 0.2 M $NaNO_3$ shows a similar reduction behavior to AB, while tetra-*n*-butyl ammonium salts split the obtained reduction into three separate waves, with the first wave being reversible. The first wave is ascribed to the radical anion of AOB, as shown by *in situ* UV-VIS spectroscopy. The second wave corresponds to the formation of the AOB di-anion. This electron-rich species is protonated, and by elimination of hydroxide, AB is formed.[20] As AB is reduced to the radical anion at potentials needed for the second AOB reduction, the formed AB is directly consumed.[21] The third

[a] D. Schatz, F. M. Schneider, Prof. Dr. H. A. Wegner
Institute of Organic Chemistry
Justus Liebig University Giessen
Heinrich-Buff-Ring 17, 35392 Gießen (Germany)
E-mail: hermann.a.wegner@org.chemie.uni-giessen.de
[b] D. Schatz, F. M. Schneider, Prof. Dr. H. A. Wegner
Center of Materials Research (ZfM/LaMa)
Justus Liebig University
Heinrich-Buff-Ring 16, 35391 Gießen (Germany)
[c] C. Burdenski, M. M. Hansmann
Faculty of Chemistry and Chemical Biology (CCB)
Technical University of Dortmund
Otto-Hahn Str. 6. 44227 Dortmund (Germany)

Supporting information for this article is available on the WWW under https://doi.org/10.1002/chem.202404001

observed wave is therefore the formation of the hydrazine from AB radical anion. The structure of the AOB and AB radicals have been studied by EPR studies thoroughly being stable in aprotic solvents.[22,23]

Similar to 4,4′-diamino substituted AB that form quinoidal structures upon oxidation, 4,4′-diamino AOBs show reversible 2e⁻oxidation, which proceeds *via* a radical cation (Figure 1).[24] The groups of Kubota and Hecht showed a convincing correlation between nonaqueous redox potentials with Hammett parameters for *para*- and *meta*-substituted AOB and 4-amino AB respectively.[10,12,24,25] Although a direct comparison of the obtained Hammett plots is not possible, as the oxidation mechanisms of 4-amino substituted diaza-compounds is different to AB, an interesting effect can be observed by comparing 4,4′-dimethylamino AB and AOB: The potential difference between oxidation and the first reduction process is considerably larger for AOB. Herein, we want to introduce AOB as a new class of compounds for energy storage in comparison to their widely known AB counterparts. As the larger oxidative redox potential could lead to a larger cell voltage, AOB could be a potential improvement for storage solutions based on diazenes.

Results and Discussion

Cyclic voltammetry (CV) measurements of 4,4′-dimethylamino AB **4a** and AOB **3a** under the same conditions (DMF and 0.2 M $TBAPF_6$) and setup, revealed very similar reduction potentials for both compounds, while the oxidation is shifted by 160 mV to more positive potentials for AOB (Figure 2). This might be surprising, as the radical anion formed during the reduction is mainly located on the nitrogen-nitrogen bond (where the oxygen substituent of AOB is located), while the quinoidal structure is distributed over the entire molecule.

To further examine AOB redox properties, CV measurements in a variety of solvents and electrolytes were conducted. The 4,4′-diethylamino AOB **3b** was employed as model substrate in 2 M concentration with 1 mM decamethylferrocene (Fc*) as an internal standard. For solvents, propylene carbonate (PC), dichloromethane (DCM), acetonitrile (ACN) and *N*,*N*′-dimethylformamide (DMF) were tested with 0.2 M tetra-*n*-butylammonium hexafluorophosphate ($TBAPF_6$). For electrolyte salts lithium bis(trifluoromethanesulfonyl)imide (LiTFSI), tetra-*n*-butylammoium tetrafluoroborate ($TBABF_4$) and $TBAPF_6$ in DMF were investigated (Figure 3). The selection of electrolytes and solvents were based on our previous work on AB as a catholyte, in which we obtained similar results.[13] For PC, an irreversible reduction was observed, which is rationalized by the nucleo-

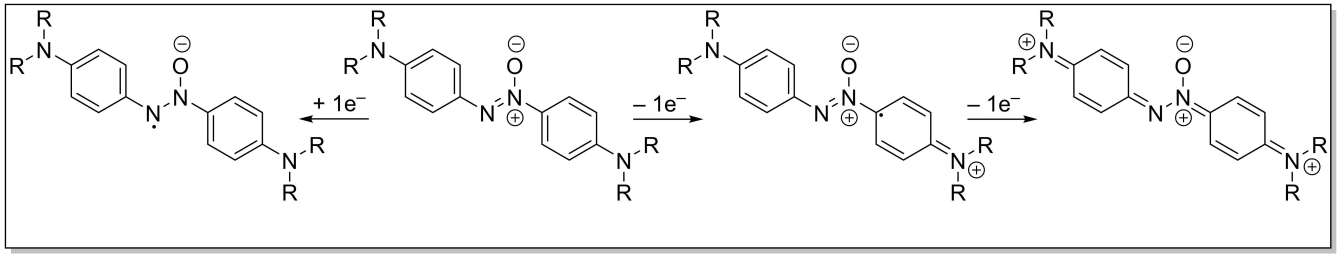

Figure 1. The 1 e⁻ reduction of AOB to a radical anion, the two subsequent 1 e⁻ oxidations affording a radical cation and the proposed bis-quinoidal structure AOB^{2+}.

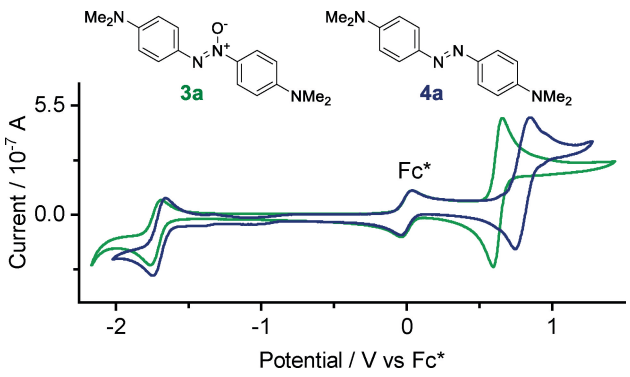

Figure 2. Cyclic voltammograms of 4,4′-dimethylamino AB **4a** (green) and AOB **3a** (blue). Solutions were prepared with 2 mM substrate, 200 mM $TBAPF_6$ and 1 mM Fc* as an internal standard in DMF. Potentials are referenced to the standard and measured with a scan rate of 100 mV/s.

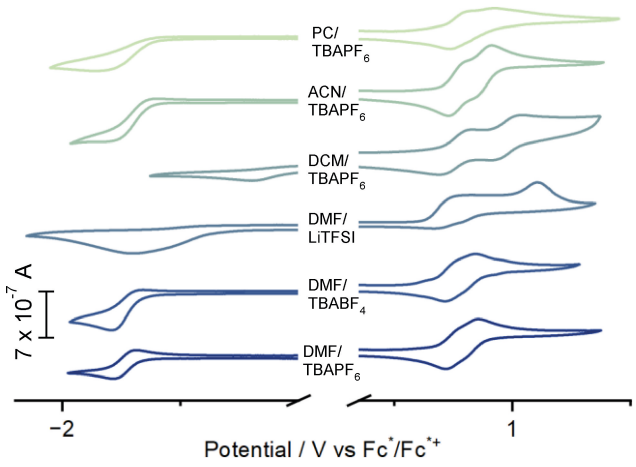

Figure 3. Cyclic voltammograms of model compound **3b** in varying solvents and with varying salts. Solutions were prepared with 2 mM **3b**, 200 mM $TBAPF_6$ and 1 mM Fc* as an internal standard. Potentials are referenced to the standard and measured with a scan rate of 100 mV/s.

philic attack of the electron-rich radical anion to the carbonate, as observed for deprotonated pyridazinones.[26] In ACN and DCM, the reduction remains irreversible, while the oxidation is noticeably split into two consecutive 1e⁻ processes. The voltage difference between these two processes is larger in less coordinating solvents, such as DCM. In the case of AB, DCM was the only solvent that allowed the observation of the two separate oxidation steps as the redox potentials of both oxidations were very close.[13] Titration experiments also proved the stepwise oxidation in ACN, though.[12] For AOB the first and second oxidation potentials are more different. Even in DMF the second oxidation is visible as a shoulder in the CV at scan rates of 0.1 V/s. By changing the electrolyte salt from a tetra-*n*-butylammonium salt to LiTFSI an additional peak appears at positive voltages. Radical anions of AOB can form cyclic dimeric complexes with alkali metals, shown by the reduction of unsubstituted AOB with $C_8H_8K_2$ in THF solutions.[27]

In the case of the more electron rich 4,4′-diethylamino AOB this complexation might be facilitated and influence the redox behavior. Changing the counter anion of the ammonium salts does not alter the appearance of the CV curves.

For AB, the resulting BF_4^- salt of the oxidized species exhibit low solubility and precipitated on the electrodes.[13] Interestingly, the oxidized AOB does not seem to precipitate from solution, which can be rationalized with the higher solubility of the employed 4,4′-diethylamino AOB **3 b** in comparison to AB **4 b**.

As the electrolyte capacity is dependent on the amount of dissolved redox active species, solubility is an important metric to optimize.[28] To improve solubility we stepwise optimized the alkyl chains from methyl to hexyl on the amine nitrogen (Scheme 1).

Nucleophilic aromatic substitution of commercially available 4-fluoronitrobenzene (**1**) with the corresponding alkyl amine was carried out at 100 °C in DMSO to yield 4,4′-dialkylamino nitrobenzenes **2 b-f**. A reductive coupling of these nitrobenzenes using Red-Al® provided the symmetrical AOBs or ABs, depending on the reaction conditions. With the minimal required equivalents of reducing agent and stirring at 0 °C, AOBs **3 a-f** were obtained in good yields. If stronger reductive conditions were used with more equivalents of Red-Al® and a short period of reflux, the AB compounds **4 a-f** were obtained in moderate yields. For ethyl AB **4 b** and AOB **3 b**, the solubility in DMF solution is 32 mg/mL and 59 mg/mL, respectively. Here, the dipole moment could be the reason why AOB has an increased solubility compared to AB, although this effect is reversed up to C_5 chains, where AOB is an oil (SI page 52). CV measurements of alkyl AB **3 a-f** and AOB **4 a-f** show the expected redox behavior of one 1e⁻ reduction and two 1e⁻ oxidations (SI page 41). The maximal peak current obtained for both redox processes, decreases for longer alkyl chains. Due to the linear relationship of the peak current and the square root of the scan rate, diffusion coefficients can be estimated using the Randles-Ševčík equation. Forward and reverse scans of the oxidation process deliver different diffusion coefficients, with the diffusion coefficients of AOB being smaller than for AB (SI page 49). The diffusion coefficient is another important metric as it plays a major part in obtainable current density and can lead to large overpotentials.[29]

As AOBs show good reversibility of the redox events independently of the scan rate, we further explored the applicability in electrochemical energy storage. As we were not able to cycle the reduction of AB, we applied AOBs only as the catholyte in charge/discharge H-cell studies. We choose the ethyl derivative **3 b** as a model substrate as it shows good solubility and can be compared to the 4,4′-diethylamino AB **4 b** that we applied earlier in galvanostatic charging cycles.[13] AOB^{2+} **3 b²⁺** was prepared *in situ* by oxidation with $NOPF_6$ and was then galvanostaticly cycled at 2 C in a symmetrical H-cell against the neutral compound (**3 b**/**3 b²⁺**). In ACN as solvent we observed a drastic capacity decay of approximately 29 % from the second to the 10th cycle (SI page 53). By electrochemical preparation of the dication, similar capacity decay was observed (SI page 55). A CV scan comparing the solution before and after cycling shows a drop in concentration of the studied compound, probably due to decomposition (SI page 54 and 56). These results are similar with the observations from AB cycling studies, indicating a related degradation mechanism for the structurally akin compounds. To evaluate the stability in ACN solution, AOB **3 b** was chemically oxidized with 2.05 eq. $NOPF_6$ in d_3-ACN to obtain the dication and analyzed by time dependent ^{1}H NMR measurements (Figure 4, and SI page 34). The ^{1}H NMR signals shift downfield similar to the ^{1}H- and ^{13}C-NMR signals of quinones in comparison to their hydroquinones. We observed no noticeable change of the observed signals even after over 6 days of being in solution at room temperature

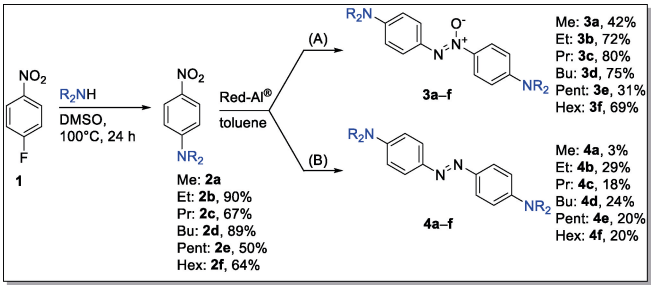

Scheme 1. Preparation of dialkylamino AOBs **3 a-f** and ABs **4 a-f**. A) 1.5 equiv. Red-Al®, 0 °C to r-t. B) 2.5 equiv. Red-Al®, 0 °C to reflux.

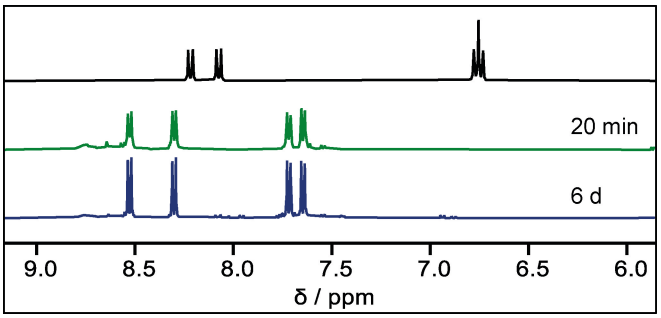

Figure 4. ^{1}H NMR spectra of AOB **3 b** (top) and after oxidation with 2.05 equiv. $NOPF_6$ in d_3-ACN over time. Depicted is only the aromatic region. (Additional spectra, see SI page 34–37)

under inert conditions. These results hint to a stable bis-quinone structure of the dication.

The product shows upon oxidation with 1.00 equiv. of oxidant a broad, unresolved EPR signal (Figure 5, left). Unlike the fully oxidized (dicationic) quinone, we observed a decrease in the intensity of the EPR signal over 2 h. This suggests only a limited stability of the formed radical species. The decline of the observed signal can be fitted by an exponential function, suggesting a second or higher order kinetic for the decomposition (Figure 5, right).

AOB **3 b** was titrated with $NOPF_6$, the change in absorbance was analyzed by UV-VIS spectroscopy and compared with a spectro-electrochemical measurement (Figure 6). That way it can be ensured, that the radical and the quinoidal structure obtained by chemical oxidation are the same as observed during electrochemical analysis. The observed maximum at 430 nm for the neutral compound AOB can be attributed to the π-π* transition, which is red-shifted compared to the corresponding AB.[30–32] Upon oxidation, the absorbance at this maximum decreases, while two new red-shifted local maxima appear at 565 nm and 706 nm.

As the intensity of these two peaks diminishes with further oxidation, they can be assigned to a radical cation intermediate. Further oxidation results in a new maximum at 455 nm, along with multiple absorption peaks around 670 nm. The red-shifted absorption is distinctly different from the oxidized form of AB, which exhibited only an absorption maximum at 380 nm.

The instability of the intermediate cation radical could explain the observed capacity decay during galvanostatic charge/discharge cycling. As the observed capacity decay is similar to that of AB, and both structurally akin compounds show similar spectro-electrochemical responses, a comparable degradation mechanism of AOB and AB can be expected.[13] The larger capacity decay of AOB in comparison to AB can be explained by the more pronounced formation of the radical intermediate, as observed by the CV scans.

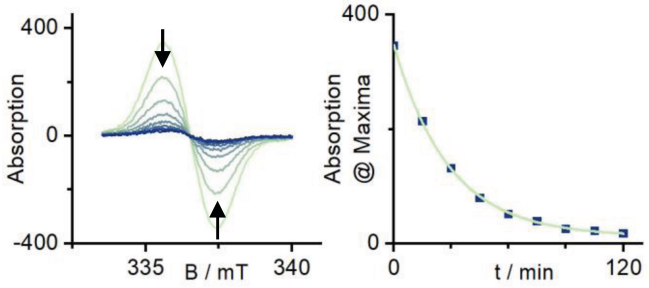

Figure 5. Left: EPR spectra of AOB **3 b** after oxidation with 1.00 equiv. $NOPF_6$ in time intervals of 15 min in ACN. Right: Decay of maximum absorption of the EPR signal over time. Fitted with an exponential decay function.

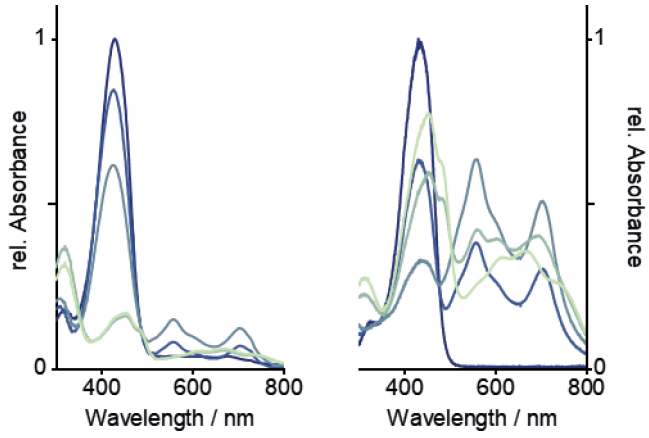

Figure 6. Left: UV-Vis absorption spectra of AOB **3 b** in ACN, titrated with $NOPF_6$. Right: Spectra resulting from a slow CV scan (0.15 V to 0.9 V with 2 mV/s vs Ag/Ag^+) in ACN with $TBAPF_6$. Increasing oxidation from blue to green.

Conclusion

We showed a first example of an 4,4'-diamino substituted AOB as a catholyte in galvanostatic charge/discharge cycles, which can be oxidized at higher potentials then the structurally similar AB. Variation of the electrolyte system split the $2e^-$ oxidation process into two distinct $1e^-$ oxidations with a radical cation intermediate. We presented the diffusion and solubility properties of different *N*,*N*'-alkyl groups. AOB shows a notable capacity decay in H-cell cycling experiments, which we assigned to the instability of the radical cation intermediate. This proposal is supported by time-dependent EPR studies, while NMR studies showed prolonged stability of the fully oxidized compound under inert atmosphere. The analysis of the product after oxidization appears to be a quinoidal dication, similar to a previously isolated product of AB oxidation. Although AOB shows an oxidation potential that is +160 mV higher than of the corresponding AB, their electrochemical instability requires further optimization for their successful application in electrochemical energy storage systems. Recently, a report presenting a skeletal rearrangement of azobenzenes to benzo[*c*]cinnolines has been published, which showed increased electrochemical stability. This strategy is also very well suitable for the AOB and will be part of future endeavours to improve the performance of AOB.[33]

Experimental Part

Exemplary Procedure for the Electrophilic Aromatic Substitution: 4-Fluoro aniline (**1**, 2.82 g, 20.0 mmol, 1.00 equiv.), K_2CO_3 (4.15 g, 30.0 mmol, 1.50 equiv.) and diethylamine (3.11 mL, 30.0 mmol, 1.50 equiv.) were stirred at 100 °C in DMSO (dry, 10 mL) under N_2 for 24 h. After cooling to r.t., H_2O (100 mL) was added, the precipitate collected by filtration, washed with H_2O (250 mL), and thoroughly dried. The solid was recrystallized from cyclohexane (approx. 10 mL to yield the product **2 b** as yellow crystals.

Yield: 3.49 g; 90 %. ^1H NMR ($CDCl_3$, 400 MHz) δ: 8.14–8.06 (m, 2H). 6.62–6.54 (m, 2H), 3.45 (q, J = 7.1 Hz, 4H), 1.23 (t, J = 7.1 Hz, 6H) ppm.

Exemplary Procedure for the Reductive Coupling to Azoxybenzenes: *N*,*N*'-Diethyl-4-nitrobenzenamin (**2 b**, 991 mg,

5.00 mmol, 1.00 equiv.) was dissolved in toluene (dry, 25 mL) and cooled to 0 °C. Red-Al® (60 %, 2.45 mL, 7.51 mmol, 1.50 equiv.) was added dropwise. The reaction mixture was stirred at 0 °C for 20 min, and at r.t. for 30 min. Afterwards, the mixture was quenched with Rusells solution, and the organic phase was washed with water (2×30 mL). The aqueous phase was extracted with EtOAc (3×60 mL) and combined with the toluene phase. Combined organic phases were washed with brine (50 mL), dried over $MgSO_4$, filtered and evaporated. The crude product was recrystallized two times from cyclohexane (approx. 15 mL) to yield the product **3 b** as a crystalline orange solid.

Yield: 617 mg; 72 %. ^{1}H NMR ($CDCl_3$, 400 MHz) δ: 8.31–8.22 (m, 2H), 8.16–8.08 (m, 2H), 6.75–6.59 (m, 4H), 3.48–3.37 (m, 4H), 1.25–1.16 (m, 6H) ppm.

Exemplary Procedure for the Reductive Coupling to Azobenzenes: *N*,*N*′-Diethyl-4-nitrobenzenamine (2 b, 991 mg, 5.00 mmol, 1.00 equiv.) was dissolved in toluene (dry, 25 mL) and cooled to 0 °C. Red-Al® (60 %, 2.00 mL, 6.25 mmol, 2.50 equiv.) was added dropwise. The reaction mixture was stirred at 0 °C for 20 min, at r.t. for 15 min, and then refluxed for 30 min. After cooling to r.t., the mixture was quenched with Rusells solution, and the organic phase was washed with water (80 mL). The aqueous phase was extracted with EtOAc (3x 60 mL) and combined with the toluene phase. Combined organic phases were dried over $MgSO_4$, filtered and evaporated. The crude product was purified by column chromatography (60 g Alox, toluene:cyclohexane 5:1, then 90 g SiO_2, cyclohexane:EtOAc 10:1) to yield the product 4 b as red crystals. Yield: 617 mg; 72 %. ^{1}H NMR ($CDCl_3$, 400 MHz) δ: 7.75–7.68 (m, 24), 6.76–6.68 (m, 4H), 3.44 (q, J = 7.1 Hz, 8H), 1.21 (t, J = 7.1 Hz, 12H) ppm.

Acknowledgements

The authors thank BMEL (Federal Ministry of Food and Agriculture) within the project FOREST (62000958) for funding, Prof. Peter R. Schreiner for providing the electrochemical cell setup, and Marcel E. Baumert for his help with H-cell measurements. We thank the Fonds der chemischen Industrie (Kekulé fellowship to C. B.). Open Access funding enabled and organized by Projekt DEAL.

Conflict of Interest

The authors declare no conflict of interest.

Keywords: azo compounds · electrochemistry · cyclic voltammetry · energy storage · radicals

[1] G. S. Hartley, *Nature* **1937**, *140*, 281.
[2] Z. Wang, P. Erhart, T. Li, Z.-Y. Zhang, D. Sampedro, Z. Hu, H. A. Wegner, O. Brummel, J. Libuda, M. Brøndsted Nielsen, K. Moth-Poulsen, *Joule* **2021**, *5*, 3116–3136.
[3] L. Zhang, Y. Qian, R. Feng, Y. Ding, X. Zu, C. Zhang, X. Guo, W. Wang, G. Yu, *Nat. Commun.* **2020**, *11*, 3843.
[4] A. Z. Weber, M. M. Mench, J. P. Meyers, P. N. Ross, J. T. Gostick, Q. Liu, *J. Appl. Electrochem.* **2011**, *41*, 1137–1164.
[5] W. Wang, Q. Luo, B. Li, X. Wei, L. Li, Z. Yang, *Adv. Funct. Mater.* **2013**, *23*, 970–986.
[6] X. Wang, J. Chai, A. Lashgari, J. J. Jiang, *ChemElectroChem* **2021**, *8*, 83–89.
[7] D. Xu, C. Zhang, Y. Zhen, Y. Zhao, Y. Li, *J. Power Sources* **2021**, *495*, 229819.
[8] X. Zu, L. Zhang, Y. Qian, C. Zhang, G. Yu, *Angew. Chem. Int. Ed.* **2020**, *59*, 22163–22170.
[9] D. Du, Y. Chen, H. Zhang, J. Zhao, L. Jin, W. Ji, H. Huang, S. Pang, *Angew. Chem. Int. Ed.* **2024**, *63*, e202408292.
[10] A. Goulet-Hanssens, M. Utecht, D. Mutruc, E. Titov, J. Schwarz, L. Grubert, D. Bléger, P. Saalfrank, S. Hecht, *J. Am. Chem. Soc.* **2017**, *139*, 335–341.
[11] E. Franz, A. Kunz, N. Oberhof, A. H. Heindl, M. Bertram, L. Fusek, N. Taccardi, P. Wasserscheid, A. Dreuw, H. A. Wegner, O. Brummel, J. Libuda, *ChemSusChem* **2022**, *15*, e202200958.
[12] A. Goulet-Hanssens, C. Rietze, E. Titov, L. Abdullahu, L. Grubert, P. Saalfrank, S. Hecht, *Chem* **2018**, *4*, 1740–1755.
[13] D. Schatz, M. E. Baumert, M. C. Kersten, F. M. Schneider, M. Brøndsted Nielsen, Max. M. Hansmann, H. A. Wegner, *Angew. Chem. Int. Ed.* **2024**, *63*, e202405618.
[14] E. Merino, *Chem. Soc. Rev.* **2011**, *40*, 3835–3853.
[15] J. M. Huang, J. F. Kuo, C. Y. Chen, *J. Appl. Polym. Sci.* **1995**, *55*, 1217–1229.
[16] H. Takahasi, T. Ishioka, Y. Koiso, M. Sodeoka, Y. Hasimoto, *Biol. Pharm. Bull.* **2000**, *23*, 1387–1390.
[17] L. Holleck, A. M. Shams el Din, *Electrochim. Acta* **1968**, *2*, 199–206.
[18] L. Holleck, S. Vavricka, M. Heyrovsky, *Electrochim. Acta* **1970**, *15*, 645–656.
[19] M. Lipsztajn, T. M. Krygowski, E. Laren, Z. Galus, *J. Electroanal. Chem. Interf. Electrochem.* **1974**, *54*, 313–320.
[20] Y. Ogata, M. Tsuchida, Y. Takagi, *J. Am. Chem. Soc.* **1957**, *79*, 3397–3401.
[21] Y. Huang, J. Lessard, *Electroanalysis* **2016**, *28*, 2716–2727.
[22] S. Jacques, G.-S. Noëlle in *PATAI'S Chemistry of Functional Groups* (Eds.: S. Patai), Wiley, **1997**, pp. 391–463.
[23] G. H. Aylward, J. L. Garnett, J. H. Sharp, *Anal. Chem.* **1967**, *39*, 457–460.
[24] T. Kubota, H. Miyazaki, M. Yamakawa, K. Ezumi, Y. Yamamoto, *Bull. Chem. Soc. Jpn.* **1979**, *52*, 1588–1596.
[25] T. Kubota, B. Uno, Y. Matsuhisa, H. Miyazaki, K. Kano, *Chem. Pharm. Bull.* **1983**, 373–385.
[26] A. Czompa, B. L. Pásztor, J. A. Sahar, Z. Mucsi, D. Bogdán, K. Ludányi, Z. Varga, I. M. Mándity, *RSC Adv.* **2019**, *9*, 37818–37824.
[27] Z. V. Todres, S. P. Avagyan, D. N. Kursanov, *J. Organomet. Chem.* **1975**, *97*, 139–144.
[28] Y. Yao, J. Lei, Y. Shi, F. Ai, Y.-C. Lu, *Nat. Energy* **2021**, *6*, 582–588.
[29] H. Wang, S. Youssef Sayed, E. J. Luber, B. C. Olsen, S. M. Shirurkar, S. Venkatakrishnan, U. M. Tefashe, A. L. Farquhar, E. S. Smotkin, R. L. McCreery, J. M. Buriak, *ACS Nano* **2020**, *14*, 2575–2584.
[30] D. L. Webb, H. H. Jaffé, *J. Am. Chem. Soc.* **1964**, *86*, 2419–2421.
[31] A. Saupe, *Z. Naturforsch. A* **1963**, *18*, 336–347.
[32] P. H. Gore, O. H. Wheeler, *J. Am. Chem. Soc.* **1956**, *78*, 2160–2163.
[33] J. Zhao, W. Zhang, D. Du, Z. Liu, W. Ji, H. Huang, S. Pang, *Angew. Chem. Int. Ed.* **2024**, e202419887.

Manuscript received: October 29, 2024
Revised manuscript received: January 21, 2025
Accepted manuscript online: January 23, 2025
Version of record online: February 10, 2025